Chapter

Charging and Discharging Mechanism of Polyimide under Electron Irradiation and High Voltage

Xiaoping Wang, Daomin Min and Shengtao Li

Abstract

Polyimide has been widely used as insulating and structural materials in spacecraft due to its excellent electrical, thermal and mechanical properties. However, its charging and discharging problem in harsh space environment has been a major limit to the development of high-voltage and high-power spacecraft. In this chapter, charging and discharging phenomena of dielectric materials under electron irradiation environment were presented. First, the electrical properties of polyimide consisting of dielectric properties, trap properties, conductivity and electrical breakdown properties were investigated, which have great influences on charging and discharging characteristics. Then, a surface charging model under relatively low-energy electron irradiation was proposed for polyimide, based on the synergistic effects of electron movement above surface and charge transport in surface layer. The DC surface flashover of polyimide under electron irradiation with different energies, fluxes and incident angles was investigated. Furthermore, a deep charging model under high-energy electron irradiation with the Fluence Model for Internal Charging (FLUMIC) spectrum was established. The effects of electron flux enhancement and operating voltage on charging characteristics were discussed in different grounding modes. It indicates that the processes of discharging under electron irradiation have a close link with the charge transport characteristics of polyimide.

Keywords: charging and discharging, charge transport, electron irradiation, high voltage, polyimide

1. Introduction

The charging and discharging of dielectric materials under space radiation environment are the main factors that cause anomalies in a spacecraft. Koons et al. counted the abnormal failures of the spacecraft, suggesting that 54.2% from the total 299 cases were caused by the charging and discharging of dielectric materials [1]. A spacecraft is inevitably exposed to space plasma, energetic particles radiation, extreme temperature, cosmic rays, etc. [2]. A situation has to be taken into consideration that partial accumulation of space charges and high electric field occur when energetic electrons penetrate through the aluminum shield and deposit in the surface or deep layer of insulating materials. When the maximum electric field of

insulating material exceeds a certain threshold, electrostatic discharge (ESD) will occur. Consequently, it will lead to the deterioration of insulating materials and even the failure of the whole electronic equipment. With the rapid increasing interest on space exploration, several countries are making efforts to build a Space Solar Power Station (SSPS) with megawatts or even gigawatts [3]. The reliability of the spacecraft becomes a very important problem. Polyimide is widely used in spacecraft system because of its good insulating, mechanical and antiaging properties [4]. Therefore, the charging and discharging mechanism of polyimide under electron irradiation and high voltage is a research focus in the field of spacecraft reliability.

Surface dielectric charging and deep dielectric charging are two kinds of dielectric charging, which are divided by the incident electron energy range and discharge position [2]. Surface dielectric charging refers to the deposition of low-energy electrons (e.g., 1–50 keV) on the dielectric surface and the induction of surface potential, while the deep dielectric charging refers to the penetration of high-energy electrons (e.g., 0.1–10 MeV) from the dielectric surface, deposition within the insulating materials and establishment of internal electric field [5]. Modeling the dielectric charging based on secondary electron yield, surface potential decay processes and characteristic parameters is the research focus in surface dielectric charging [2, 6–10]. While for deep dielectric charging, the charge transport properties of insulating materials irradiated by energetic electrons are key issues, and several models have been proposed to investigate it [11–14]. There are two types of typical models: the radiation-induced conductivity (RIC) model and the charge generation-recombination (GR) model. RIC model describes the transport processes of electrons in insulating materials under the irradiation of electron beam. It is a macroscopic model in which the parameters are given by the measurement of radiation-induced conductivity [14]. GR model describes the generation and recombination processes of electron-hole pairs in insulating materials. It is a microscopic model in which some specific parameters are difficult to be determined.

Charge behavior on the dielectric surface layer or the deep layer under electron irradiation has an important influence on discharging properties. As to DC surface flashover, it implies that the essence of surface flashover is the charge transport behavior across gas-solid interface under high electric field, which involves charge trapping and de-trapping properties in dielectric surface layer, secondary electron emission properties, impact ionization of gas molecules and electron multiplication properties in gaseous phase (or desorbed gas). The development process and formation of surface flashover is a coupling effect of the above factors. The vacuum surface flashover voltage of dielectric material irradiated by electrons is much lower than that in vacuum or gaseous atmosphere. At present, several theories have been postulated to explain the surface flashover phenomenon in vacuum, among which the theory of secondary electron emission avalanche (SEEA) is dominant [15]. The flashover of insulating material in vacuum under electron beam irradiation is also closely related to the field-emission electrons emitted from the cathode-dielectric-vacuum triple junction (CTJ) and secondary electrons (SE) [16]. A large number of experimental studies emphasize the effects of deposited charges in the dielectric surface layer, while few data can be obtained about the effect of kinetic electron from the electron beam on surface flashover [17]. On the aspect of dc electrical breakdown mechanism of polyimide, it has been proven that under the action of a high electric field, charges are injected into the insulating materials, and space charges are accumulated [18–20]. The electric field distortion appears inside the insulating materials caused by the accumulated space charges. When the maximum local electric field exceeds a threshold value, the electrical breakdown will occur [19, 21].

In this chapter, the charging and discharging phenomena of dielectric materials under electron irradiation environment were introduced. The electrical properties

of polyimide were investigated. The surface and deep charging process and model of polyimide radiated by electrons were analyzed. Then, the experimental results of DC surface flashover during electron irradiation with different energies, fluxes and incident angles were investigated.

2. Charging and discharging phenomena of dielectric materials under electron irradiation environment

2.1 Charging and discharging phenomena and hazards

In the field of spacecraft charging and discharging, the potential of the spacecraft is relative to the zero potential of the space plasma. Although the density of space plasma is fluctuating, it is much faster than the change of the spacecraft potential on the time scale. The spacecraft potential is floating. The spacecraft operates in a harsh space environment, such as plasma, high-energy electrons, atomic oxygen, etc., and charging and discharging phenomena will occur in the surface or deep layer of the spacecraft [2]. **Figure 1** depicts a schematic diagram of the spacecraft floating potential.

When the energy of the incident particles is low, the charge exchange process will appear between spacecraft and the surrounding environment. Environmental electrons or ions interacting with target atoms on the surface of the dielectric material will generate the secondary electrons and backscattered electrons. In addition, when the spacecraft is operating on the sunny side, photoelectrons are generated on the surface of the dielectric material. The combined effects of the above processes will cause charging and discharging phenomena on the surface of the dielectric materials. For different dielectric materials, due to their different secondary electron emission coefficients, backscattering coefficients and photoelectron coefficients, the surface charge exchange processes are different. Consequently, different surface potentials appear on the dielectric materials, which will cause unequal charge between the dielectric materials [2].

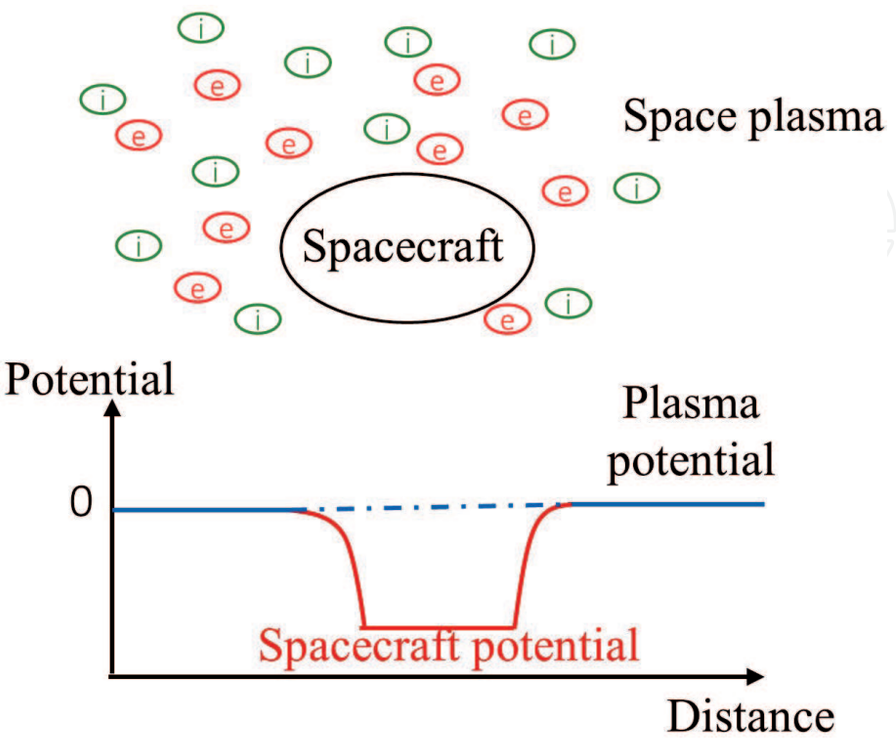

Figure 1.
The schematic diagram of spacecraft floating potential in space plasma environment [2].

The deep dielectric charging refers to the process that high-energy electrons (MeV) penetrate through the dielectric surface and deposit within the insulating materials [22]. Incident electrons penetrate into insulating materials, and their energy will gradually transfer into target atoms, owing to the physical mechanism of elastic scattering or inelastic scattering. For high-resistivity polymer, the intrinsic conductivity is very low. High-energy electrons penetrate the surface and deposit inside the material. These charges are called deposited electrons. Under the radiation of the space electron spectrum, electrons of different energies have different penetration distances inside the material, resulting in the formation of deposited charge layers of different depths. The charge accumulation will cause distortion of the electric field, which is likely to cause internal electrical breakdown of the dielectric materials [23].

From 1980 to 2005, the statistics of 156 anomalies of orbiting spacecraft showed that 45% of spacecraft anomalies were caused by the failure of the power system of the spacecraft [24], among which the insulating materials and structure of solar array and its drive assembly are most likely to discharge. The spacecraft power system fails once the solar array or its drive assembly fails. Even worse, the spacecraft will be out of control. A Nigerian satellite launched by China in November 2008 completely failed due to the failure of solar array drive assembly [25]. Especially with the increase of spacecraft operating voltage and power requirements, the coupling effect of high operating voltage and space radiation environment will pose a greater threat to the insulation system of spacecraft.

2.2 Research process of dielectric charging and discharging

As early as the 1920s, Mott-Smith and Langmuir began the initial theoretical exploration of the electrostatic charging of isolated bodies in space [2]. With the launch of the first artificial satellite in 1957, humankind entered the era of space, and the related issues of space dielectric charging have gradually attracted researchers' attention. Before 1980, it was believed that the charging and discharging of the dielectric surface was the main cause of spacecraft anomalies, and related research focused on the surface charging phenomenon [26]. With the occurrence of abnormal spacecraft failures and the launch of CRRES satellite (Combined Release and Radiation Effects Satellite) in the 1990s, deep dielectric charging of the spacecraft came into focus and research on spacecraft charging entered a new era [27]. H.B. Garrett published two review papers in 1981 and 2000 [26, 27], which summarized the research progress of spacecraft surface charging before 1980 and research development of surface charging and deep charging between 1980 and 2000. Lai published a review paper in 2003 [28], which summarized the suppression methods of dielectric charging.

Since the twenty-first century, great achievements have been made in space environment exploration, basic theoretical research and ground simulation experiments. However, the charging and discharging of dielectric materials is still the main factor threatening the safe operation of spacecraft. Especially with the development of high-voltage and high-power spacecraft, the field of dielectric charging and discharging is facing new challenges.

3. Electrical properties of polyimide

3.1 Dielectric properties

The complex permittivity of polyimide with thickness of 100 μm was measured at room temperature using a broadband dielectric spectrometer (Concept 80, Novocontrol Technologies, Germany). The applied voltage was 1 V_{rms} and the

frequency was from 10^{-2}–10^{5} Hz. **Figure 2** depicts the real and imaginary parts of the relative complex permittivity, obtained from polyimide sample at room temperature, which is a function of frequency in semi-logarithmic coordinates [29]. **Figure 2** shows that the real part of relative complex permittivity increases slightly as frequency decreases. In the frequency range of 10^{-2}–10^{5} Hz, the imaginary part is lower than 3.6×10^{-3}. The small dielectric relaxation strength of the relaxation peak around 30 Hz reveals that the dipolar moment is very low. The dielectric loss, $\varepsilon''/\varepsilon'$, is very low, which indicates that in the dc electrical breakdown experiments at room temperature, the Joule heating generated by the dipole orientation is negligible [29].

3.2 Bulk and surface trap properties

Thermally stimulated depolarization current (TSDC, Concept 90, Novocontrol technologies, Germany) was carried out on a polyimide sample with a thickness of 100 μm to investigate its trap distribution characteristics. **Figure 3** shows the results of TSDC experiments for polyimide [29]. Thermally stimulated relaxation processes can be observed in the temperature range of 10–170°C. One obvious relaxation peak is around 69°C, while another relaxation peak may be located near 135°C. The experimental results were analyzed using the classical TSDC theory to reveal the thermally stimulated processes and their activation energies [30].

The TSDC experimental results were fitted and four relaxation peak components could be obtained. As shown in **Figure 3**, it can be seen that the fitting results are in good agreement with the experiments. We can determine the peak temperature, activation energy and relaxation time for the four relaxation processes listed in **Table 1**. The activation energies of four peaks at 69, 87, 109 and 135.5° are 0.60, 0.65, 0.70 and 0.83 eV, respectively. As the temperature at the relaxation peak increases, the corresponding activation energy increases. The three peaks at 69, 87 and 109°C may correspond to shallow traps that assist carriers hopping process in polyimide, while the peak at 135.5°C may correspond to deep traps that can capture mobile carriers and accumulate space charges. The energy of deep traps is

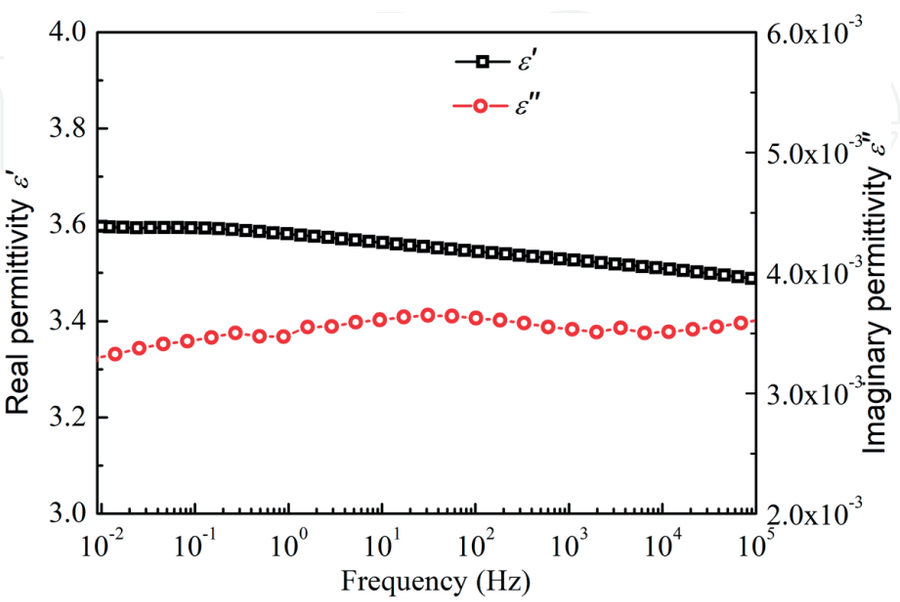

Figure 2.
The real and imaginary parts of relative complex permittivity, ε' and ε'', of polyimide as a function of frequency at room temperature [29].

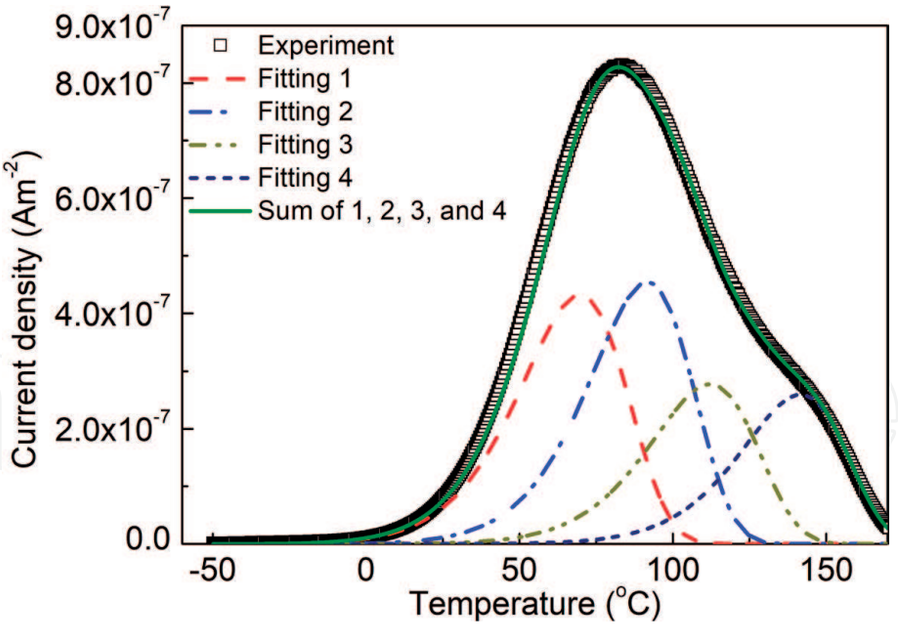

Figure 3.
TSDC experimental results of polyimide after being polarized at an applied voltage of 250 V at 180°C for 30 min. The classical TSDC theory was used to fit the experimental results. Symbols and solid curves represent experimental and fitting results, respectively [29].

Peak temperature (°C)	E_A (eV)	B (Am^{-2})	τ_0 (s)
69	0.60	2.63×10^{-4}	7.50×10^{-7}
87	0.65	2.01×10^{-4}	4.23×10^{-7}
109	0.70	1.80×10^{-4}	3.23×10^{-7}
135.5	0.83	1.60×10^{-4}	3.09×10^{-8}

Table 1.
Parameters for relaxation processes extracted from TSDC experimental results [29].

consistent with the results obtained from the Arrhenius relation between conductivity and temperature [4].

Surface potential decay was carried out on a polyimide sample under electron radiation to investigate its surface trap distribution characteristics. In this experiment, charging process takes a very short time, about 25 s, as the electron flux density was so high. We set that with a filament emission current of 10 μA and a radiation distance of 300 mm, and the charging process was completed within 30 s. After radiating for 30 s, we turned off the electron gun and then moved the probe over the sample to measure the surface potential. **Figure 4(a)** gives the surface potential decay curves of polyimide under electron radiation of different energy levels (3–11 keV) [31].

It can be seen that the initial surface potential gradually increases with the increase of electron energy. This indicates that the charging process and properties are different under electron radiation of different energy levels. Hence, the dielectric properties during the charging process can be investigated by analyzing the initial surface potential of the dielectric after the charging process.

The surface trap distribution of polyimide can be obtained from surface potential decay model, as shown in **Figure 4(b)** [31]. There are two types of traps, defined as shallow and deep traps, respectively. It can be seen that the trap charge density related to shallow traps is more than that of deep traps under the

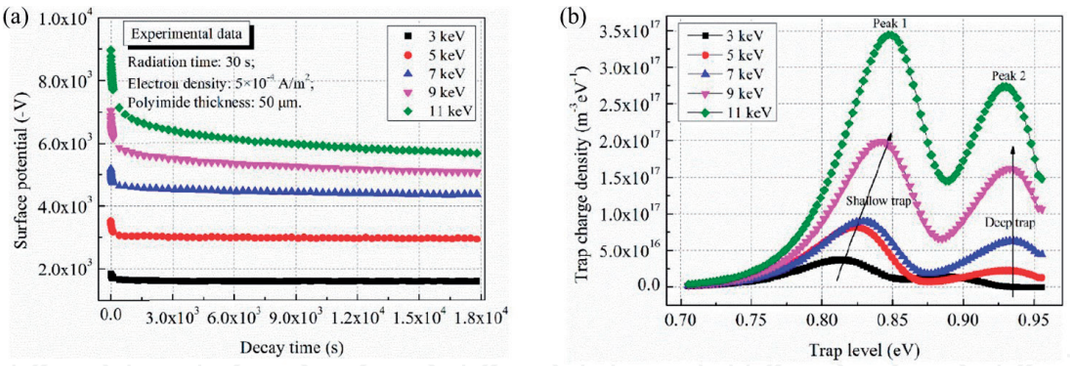

Figure 4.
Surface potential decay curves (a) and surface trap distributions (b) of polyimide after irradiation by electron beam with different energies [31].

same electron energy radiation. The charges captured in relatively shallow traps can escape the trap center in a short interval, which is demonstrated by the rapid decay of surface potential. With the time increases, these de-trapped electrons will migrate to the grounded electrode under the effect of the internal electric field. By contrast, deeply trapped charges remain in the trap center for a longer period. The density of deep traps determines the steady surface potential, and the stabilization time depends on the energy level of the deep traps.

The surface trap distribution of polyimide presents different behavior under radiation from electrons of different energy levels. The shallow trap level increases slightly with the increase of electron energy, while the deep trap level remains unchanged about 0.94 eV. Under the radiation of different electron energy, the depth of the electron deposition layer and the range of electrons are different. The higher the electron energy, the deeper the deposition layer. These trapped charges need to overcome a much higher potential barrier to escape the trap center. Therefore, the shallow trap energy level increases with the gradual increase of the electron energy. In addition, the total trap charge density gradually increases with increasing electron energy. Due to the increased electron energy, the distance from the electron deposition layer to the dielectric surface is longer, and much more charges will be captured by the trap centers [31].

3.3 Shallow trap-controlled carrier mobility and conductivity

The surface potential experimental results of samples charged by negative corona discharging and positive corona discharging as a function of time are shown in **Figure 5** [29]. Negative and positive charges are deposited on the surface of polyimide, and electric field is established inside the polyimide during the charging process. After charging, surface charges are injected into polyimide, and the migration of charges toward the grounded electrode in the bulk leads to the decay of surface potential. The decay rate of surface potential varies before and after the injected charge carriers flow out of the dielectric material, as shown in **Figure 5** [29]. The time when the front charge carriers arrive at the grounded electrode is defined as transit time t_T. The transit point existing at the beginning of the potential decay curve can represent the mobility of carriers controlled by shallow traps [29]. In order to obtain the transit time t_T, the potential decay results were fitted by an exponential function, and then we obtained the relation between $t\mathrm{d}\phi_s/\mathrm{dt}$ and t. The time corresponding to the peaks can be regarded as transit time t_T, and it is used to calculate carrier mobility controlled by shallow traps according to the following Eq. (1) [29, 32]:

$$\mu_{0(e,h)} = d^2/\phi_{s0}t_T \quad (1)$$

Here, μ_0 is the carrier mobility controlled by shallow traps in $m^2V^{-1}s^{-1}$, d is the thickness of sample in m, and ϕ_{s0} represents the initial surface potential in V. The subscripts have the following meaning: (e) for electrons and (h) for holes. By calculation, the hole and electron mobilities controlled by shallow traps are 1.80×10^{-14} and 3.67×10^{-14} $m^2V^{-1}s^{-1}$, respectively.

For studying the surface and volume charge transportation properties, the isothermal surface potential decay (ISPD) experiment on space-grade polyimide was carried out at various temperatures from 298 to 338 K. In high vacuum, the charge was accumulated on the surface of polyimide under low-energy electron irradiation. After irradiation, the charge was transferred to the grounding electrode on the surface through the volume. Through the three parameters of surface resistivity, volume ohmic resistivity and charge carrier mobility, the leakage rate of electron was determined. And the three parameters were revealed by a two-dimensional ISPD model established by using genetic algorithm (GA), as shown in **Figure 6** [33].

As shown in **Figure 6**, the carrier mobility increased with temperature, while the surface resistivity and volume ohmic resistivity of polyimide decreased with temperature. The surface resistivity, volume ohmic resistivity and carrier mobility were obtained. For example, at 298 K, they were 1.02×10^{19} Ω, 2.87×10^{17} Ω m and 1.49×10^{-19} m^2/V s, respectively. The calculated errors were all not more than 0.9%, which showed that there was a good consistency between the experimental and simulated 2D ISPD results [33].

3.4 Electrical breakdown properties

The influencing mechanism of sample thickness on electrical breakdown of polyimide is not very clear until now. The dc electrical breakdown fields of polyimide films with different thicknesses from 25 to 250 μm were measured using a computer-controlled voltage breakdown test device. The dc electrical breakdown experiments were carried out under 30°C using spherical copper electrodes with a diameter of 25 mm in transformer oil. The rate of dc voltage increase is 1 kVs^{-1}. For

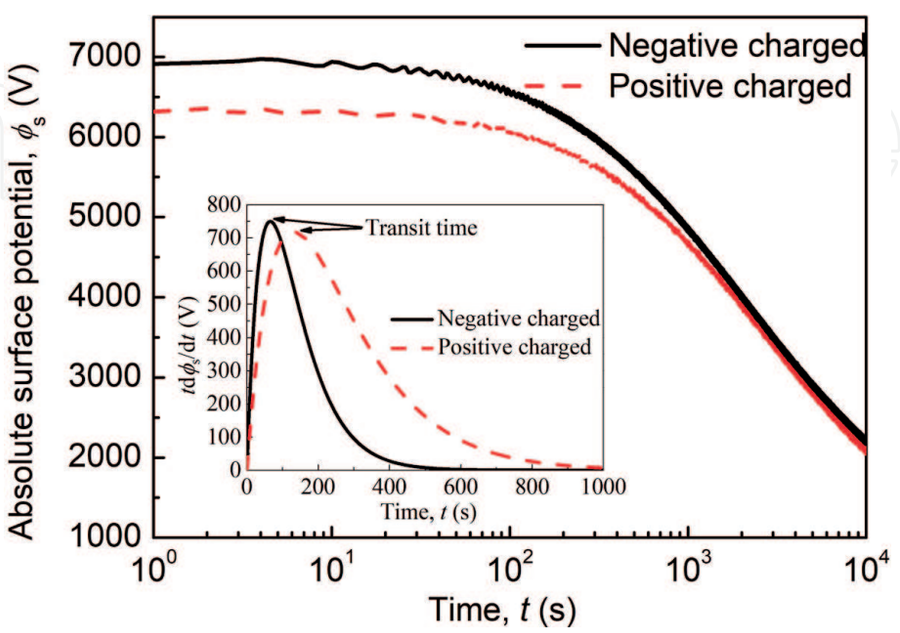

Figure 5.
Surface potentials of polyimide charged by negative corona discharging and positive corona discharging as a function of time at room temperature [29].

each thickness of the sample, at least 15 times breakdown tests are performed. The average value of all data is taken as the breakdown electric field of the sample.

Figure 7 shows the experimental results of the dc electrical breakdown field of the polyimide film, F_b, as a function of thickness, d, at room temperature [29]. As shown in **Figure 7(a)**, the dc electrical breakdown field of polyimide films decreases with an increase in sample thickness. In addition, the derivative of dc electrical breakdown field with respect to sample thickness dF_b/dd decreases with the increase in sample thickness. The relation between the dc electrical breakdown field and sample thickness looks like an inverse power function. Accordingly, we change the linear coordinates in **Figure 7(a)** to double logarithmic coordinates in **Figure 7(b)**. It can be seen from **Figure 7(b)** that the dc electrical breakdown field of polyimide is linear with sample thickness under double logarithmic coordinates [29].

The influence of sample thickness on polymer breakdown can be explained by electron avalanche breakdown, electromechanical breakdown, free volume breakdown and space charge modulated electrical breakdown [29, 34]. In electron avalanche breakdown, the energy gain of electron can be obtained by free electron movement in the conduction band of dielectric material under the action of electric field [34]. When the energy exceeds the band gap energy, the electrons in the valence band may be excited to the conduction band, resulting in the chemical bond breaking. The avalanche effect is caused by further collision and ionization of the released electrons with other matrix atoms, which results in the doubling of local current and finally triggers the breakdown. The electric breakdown field decreases

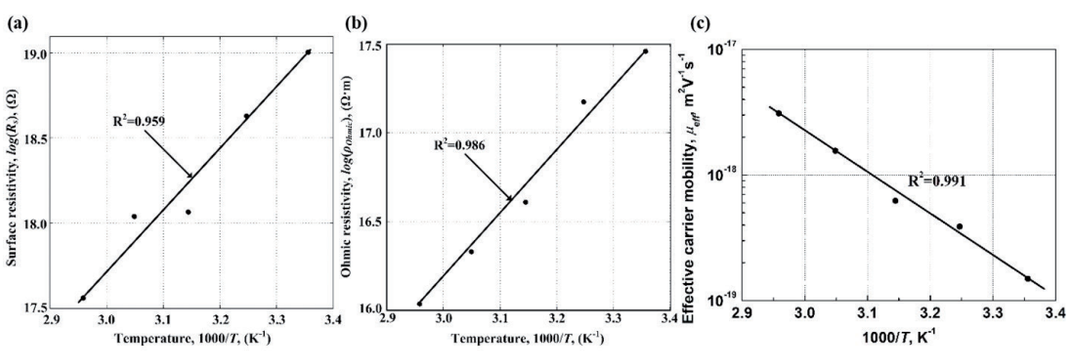

Figure 6.
Arrhenius plot of surface resistivity (a), volume ohmic resistivity (b), and charge carrier mobility (c) of polyimide. The linear fitting errors, R^2, were respectively 0.959, 0.986 and 0.991 from (a) to (c) [33].

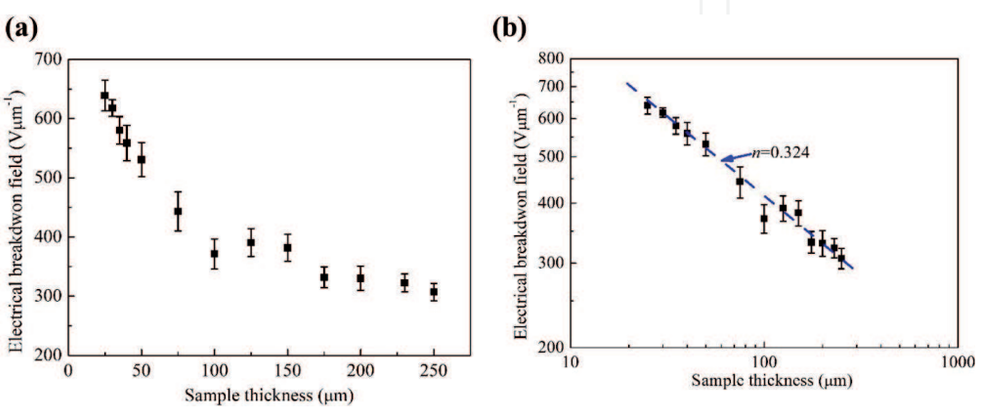

Figure 7.
Experimental results of dc electrical breakdown field of polyimide at various thicknesses in linear coordinates (a) and in double logarithmic coordinates (b) [29].

with the increase of sample thickness, which is due to the critical number of electrons produced in the whole sample thickness by collision ionization [29, 34]. The Stark-Garton model of mechanical and electrical breakdown has been widely used to predict the breakdown strength of thermoplastics, while the Young's modulus and dielectric constant of temperature-sensitive polymers determine the mechanical and electrical breakdown strength [34]. Because the thickness of the sample determines the electrostatic compressive stress and the opposite elastic stress produced by the electrostatic attraction of the two electrodes, the electric breakdown field is a decreasing function of the sample thickness. In the theory of free volume breakdown, it is assumed that the electric breakdown field of polymer depends on the longest mean free path of electron. Electrons are accelerated in the free volume, and their average free path depends on the maximum length of the free volume. When enough energy is obtained by electrons in the free volume to overcome the potential barrier, the local current will be multiplied, so that the material is heated to a very high temperature and finally causes the phenomenon of electrical breakdown. From a statistical point of view, the longest free path is a function of sample size, so the electric breakdown strength is related to sample thickness.

4. Surface charging and discharging mechanism of polyimide

4.1 Surface charging process and model of polyimide radiated by low-energy electrons

The synergistic effect of surface electron movement and charge transport in dielectric surface layer should be taken into account when studying the charging process under low-energy electron radiation (1–50 keV). A schematic diagram of charge transport on polyimide surface and in its surface layer under low-energy electron radiation is shown in **Figure 8**. 'Surface layer' refers to the area inside the material that is about a few micrometers from the surface of the dielectric material.

The intrinsic conductivity of polyimide with high resistivity is very low, but its total conductivity will increase due to the radiation-induced conductivity (RIC). The incident electrons are mainly deposited in a dielectric surface layer of about a few microns [16], and they will migrate to the interior of polyimide. However, the charge in the surface layer will continue to be accumulated, because the charge conduction velocity is far lower than that of deposition [5].

The surface potential is very low in the initial stage of electron radiation, whose reverse effect on the incident electron energy is very weak. Rather than being released by the secondary electrons, the incident electrons will be deposited on the surface. On the one hand, the change of the distribution of the deposited electrons in the surface layer and the change of the charge transfer characteristics occur due to the change of the incident electron energy and density on the dielectric surface, and it will further affect the negative potential and the induced reverse electric field on the surface in turn. On the other hand, these deposited electrons will generate an internal electric field, whose intensity will gradually increase with the radiation duration. A reverse-acting force will be produced by this field on the moving electrons reaching the dielectric surface [16]. As a result, the incident trajectory and the kinetic energy of the incident electron can be changed by the reverse electric field, by which the secondary electron yield characteristics of dielectric surface will be greatly affected.

The charging process will be stable, if the incident electron current is equal to the sum of the conduction current in the surface layer and the secondary electron generation current on the surface. Therefore, the key to the study of the charging

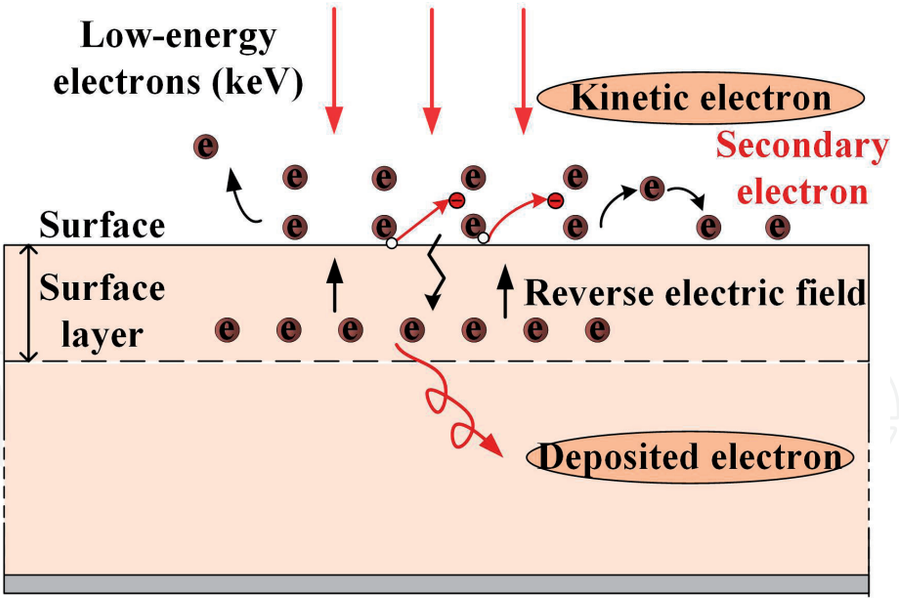

Figure 8.
Schematic diagram of charge transport on polyimide surface and in the surface layer under low-energy electron radiation [31].

process is a thorough understanding of the charge transfer properties in the dielectric surface layers and kinetic electrons in the surface [31].

4.1.1 Surface kinetic electron properties

A reverse electric field will be formed in the process of electron radiation by the electrons accumulated in the polyimide surface layer, by which the trajectory of the incident electrons will be changed, and thus there will be a dynamic impact on the density and energy of the electrons reaching the polyimide surface. The characteristics of the subsequent incident electrons are different from those of the initial electrons. They will change with time, thus affecting the yield attributes of the surface secondary electrons. **Figure 9(a)** gives the energy and density of electrons reaching the polyimide surface over radiation time. **Figure 9(b)** shows the current density of secondary electrons emitted from polyimide surface and the surface conduction current against time [31].

Due to the repelling effect from the electric field forming in the surface layer, with the radiation time increasing, the energy and density of electrons reaching the polyimide surface gradually decrease, as shown in **Figure 9(a)** [31]. It can also be observed that, with radiation time increasing, the energy and density of electrons reaching the polyimide surface become a whole range of values from single values, resulting in a great impact on the dynamic processes of secondary electron movement and electron deposition, transport and accumulation behavior in the dielectric surface layer. Secondary electron yield coefficient gradually increases with the drop of the energy of kinetic electrons reaching the polyimide surface, and correspondingly the secondary electron yield current gradually increases, as shown by the red curve in **Figure 9(b)** [31]. In addition, the phenomenon that some of the incident electrons deposit in the surface layer after penetrating the dielectric surface will occur, especially at the initial stage. With different radiation time and material position, the distributions of deposited electrons are different. The change of charge conduction current density on the polyimide surface is shown by the blue curve in **Figure 9(b)** [31]. In the initial radiation stage, the charge conduction process can be overcome by most of the incident electrons under the radiation-induced conductivity, after they penetrate the dielectric surface. On the contrary,

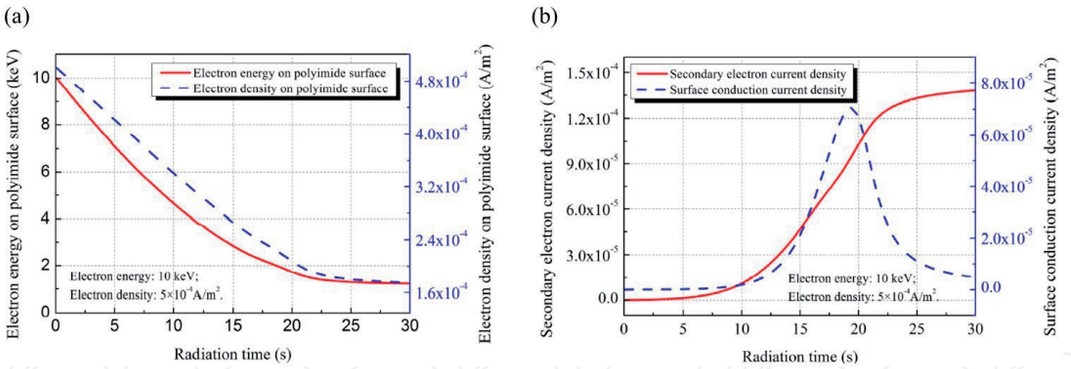

Figure 9.
Surface kinetic electron properties. (a) The energy and density of electrons reaching the polyimide surface over the radiation time and (b) secondary electron emission and charge conduction on polyimide surface over the radiation time [31].

the production process of secondary electron is very weak. The secondary electron yield current increases with the energy of the kinetic electron to the surface of polyimide decreasing over radiation time. With the radiation time increasing, the conduction current density on the polyimide surface will gradually decrease, resulting in most of the incident electrons on the polyimide surface being released by the secondary electrons, and only a few electrons penetrating the surface. In the case of low-energy electron radiation, the influence of secondary electron generation process is more obvious than that of deposition electron transport process. The dynamic process of charge transport in the dielectric surface layer plays a leading role in the initial stage of radiation, so it cannot be ignored [31].

4.1.2 Charge transport properties in the surface layer of polyimide

A non-uniform distribution of potential and electric field is caused by the different spatial distribution of charge in polyimide surface layer under low-energy electron radiation. By solving charge balance equation, current conduction equation and Poisson equation, the distribution of electric potential and electric field can be obtained. **Figure 10(a)** and **(b)** depicts the spatial and temporal distributions of the internal potential and electric field of polyimide under electron radiation. The electron energy is 10 keV and the flux density is 5×10^{-4} A/m^2.

Figure 10(a) shows that with the radiation time increasing, the surface potential increases gradually, and the maximum potential appears at about 25–30 s. Meanwhile, with the material depth increasing, the potential decreases. It can be seen in **Figure 10(b)** that the electric field intensity increases with the radiation time increasing, which is due to the electrons accumulating in the polyimide surface layer. The electric field tends to be stable when the radiation time is more than 25 s. It can be obtained that the electric field decreases gradually from the maximum electron range to the dielectric surface, on which the electric field is equal to zero, according to Poisson's equation. The distribution of the maximum potential and the maximum electric field over the radiation time is depicted in **Figure 10(c)**. It can also be seen from **Figure 10(c)** that the maximum surface potential increases with the radiation time increasing and tends to stabilize at 25–30 s. When the radiation time is 30 s, the stable potential reaches −8778 V. The corresponding experimental result that was measured by the non-contact surface potentiometer was −8424 V, which is slightly lower than the simulated value. Correspondingly, the maximum electric field is 1.78×10^8 V/m, which is very high, but does not cause damage to the material. Once electron radiation stops, the electric field value will drop sharply.

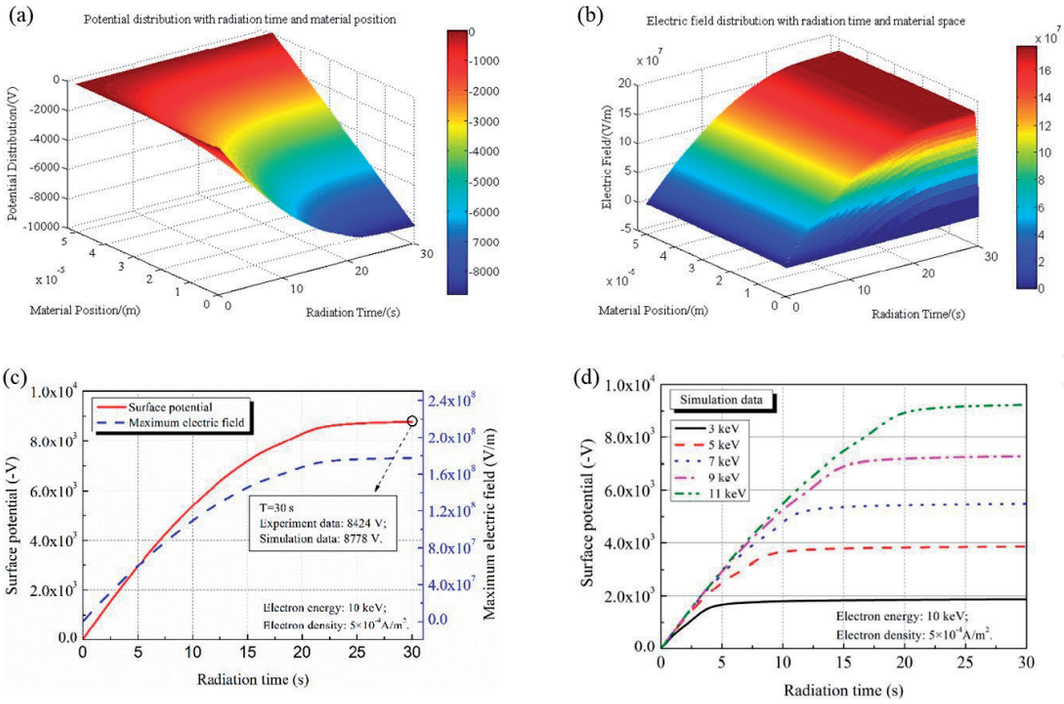

Figure 10.
Charge transport properties in polyimide surface layer. Distributions of internal potential (a) and internal electric field (b) at various material positions and radiation times. Maximum potential and maximum electric field (c) and surface potential (d) as a function of radiation time [31].

Figure 10(d) shows the distribution of surface potential with over the radiation time under different incident electron energy levels [31].

4.2 DC surface flashover mechanism of polyimide irradiated by electrons

Li et al. measured the DC surface flashover voltage of insulating material in vacuum under electrons irradiation by controlling the energy, emission flux and incident angle of the electron beam [16, 35]. Combining the common effects of deposited electrons and kinetic incident electrons, they proposed a physical model of surface flashover under electrons irradiation.

Figure 11(a)–(c) depicts the effect of electron energy, incident angle and electron flux on DC surface flashover voltage of polyimide during electron irradiation. The surface flashover voltage of polyimide irradiated by electron beam is determined not only by the deposited electrons in the surface layer of the dielectric but also by the kinetic incident electrons striking the dielectric surface [35].

During low-energy electron irradiation, for one thing, deposited electrons will reduce the electric field in the vicinity of CTJ; thus, the field-emission effect is suppressed, hindering the initiation of SEEA. For another, the surface potential established by deposited electrons is proportional to the electron energy. The secondary electrons will be repelled away from the polyimide surface, hindering the development process of SEEA. Both of these two effects will promote the surface flashover voltage.

However, during high-energy electron irradiation, the kinetic incident electrons will strike the polyimide surface to generate secondary electrons, which promotes the development of SEEA. If the impact points of kinetic incident electrons are close to the CTJ, they will be an alternative to field-emission electrons as the seed of SEEA. Thus, a high voltage to generate field-emission electrons and initiate the SEEA is no longer needed. A lower applied voltage can provide energy for secondary

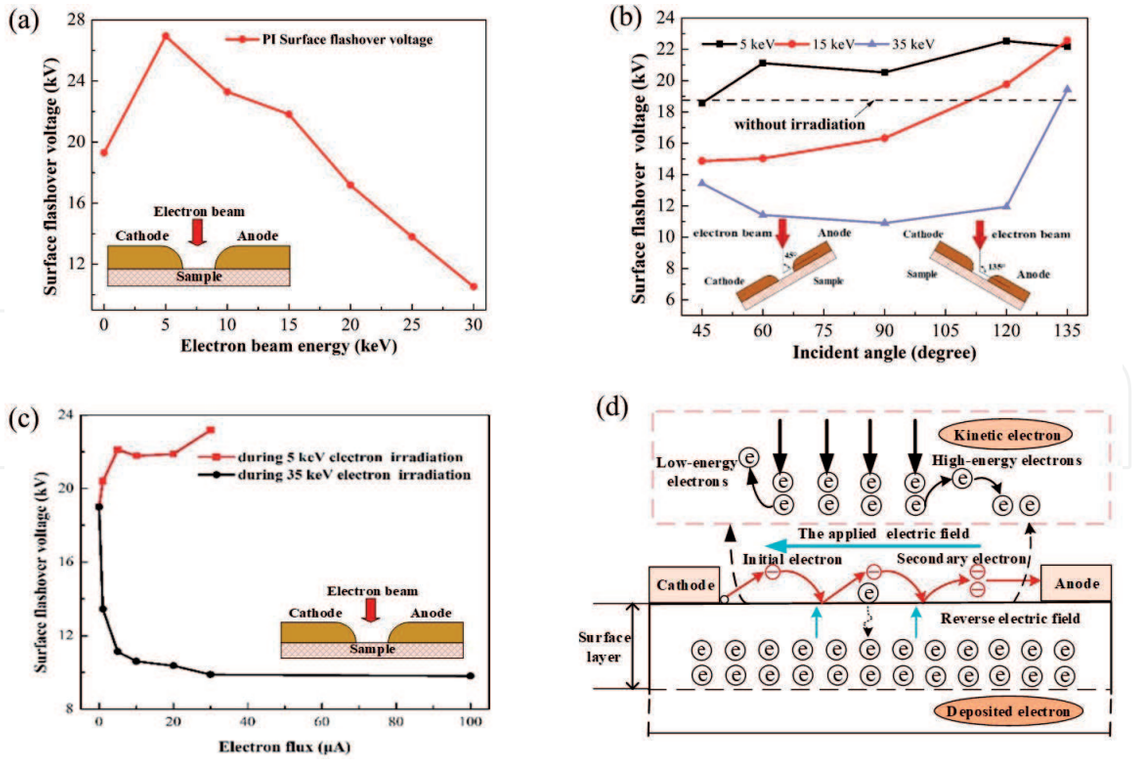

Figure 11.
DC surface flashover properties of polyimide under electron irradiation. Effects of electron energy (a), incident angle (b), and electron flux (c) on surface flashover voltage. (d) The surface flashover model for dielectric materials under electron irradiation [35].

electron multiplication. In other words, the applied voltage for electron multiplication is much lower than that for the field-emission–initiated SEEA. For another, the electron beam bombardment will release the adsorbed gases on the irradiated area of polyimide surface. Considering the shielding effect of the cathode, when the applied voltage is the same value, the irradiated area of the case during high-energy electron beam irradiation is larger than that of the case during low-energy electron beam irradiation. When enough adsorbed gases are released, ionization may be caused by electron beam bombardment as well as secondary electrons that gain enough energy from the applied electric field. If the electron beam can approach the polyimide surface, the effects of deposited electrons will be suppressed by those kinetic incident electrons. The model of surface flashover under electrons irradiation is shown in **Figure 11(d)** [35].

5. Deep charging and discharging mechanism of polyimide

5.1 Deep charging model of polyimide radiated by electrons

Energetic electrons are difficult to conduct when they are deposited inside polyimide due to its low conductivity, resulting in deep charging of insulation. Under the condition of typical electron radiation environment in geosynchronous orbit (GEO), deep charging of polyimide normally does not cause discharge risk. However, during the energetic electron storm, the electron flux will increase by 2–3 orders of magnitude within a few days and last for 10 days or so. At this point, the incident electron flux will exceed the threshold of 0.1 pA/cm^2, resulting in a great risk of ESD [5, 36].

FLUMIC model, proposed by Rodgers et al., based on spacecraft data of GOES/SEM and STRV-1b/REM was utilized in this paper to manifest the electron radiation

environment in GEO [37, 38]. It is commonly agreed that FLUMIC model is suitable for charging risk assessment and spacecraft design due to its complete demonstration of seasonal and annual variations in energetic electron flux. **Figure 12(a)** depicts FLUMIC spectrum under typical and extreme space environment [36].

The penetration depth of energetic electrons in polyimide can be obtained from the Weber semi-empirical equation. The charge conduction process consists of inherent charge conductivity and radiation-induced conductivity. Charge transport process satisfies the current conduction equation, the charge continuity equation and Poisson's equation [36].

Assume that electrons irradiate a plate polyimide from the upper side. HV is applied to one side of the sample, and the other side is suspended or grounded. Four cases of the sample are considered altogether, that is, (A) suspended-HV; (B) HV-suspended; (C) grounded-HV; and (D) HV-grounded, as shown in **Figure 12(b)** [36]. The condition before the hyphen indicates condition on the upper surface, and the latter indicates condition on the lower surface.

Here, the first case will be discussed: HV is 0 V, that is, and the electrode is grounded. Case A becomes suspended-grounded, case B becomes grounded-suspended, and cases C and D are merged into grounded-grounded. We take the condition with enhancement of 100 and radiation time of 5 days for an example.

5.2 Simulation results and discussion

In case A, the maximum electric field strength reached 5.00×10^7 V/m, appearing near the lower electrode. Most of the charge deposited near the radiated surface, though part of the charge mitigated toward the lower electrode driven by the electric field, as shown in **Figure 13(a1)–(a3)** [36]. In case B, the maximum electric field strength reached 4.39×10^7 V/m, appearing near the upper electrode. Vast charges are accumulated at the region near the radiated surface. As **Figure 13(b1)–(b3)** shows, compared with case A, the electric field in case B tends to move downward, inhibiting the migration of electrons from the field to the bulk of sample, which leads to deposition of the charges near the surface and formulate a local high-space charge area [36]. When both electrodes are grounded, it is clear that, similar to the results in case B, the electric field near the upper electrode is at a lower position vertically, restricting the transformation of the electrons to the bulk of the sample and electrons accumulated at the region near upper electrode. In addition, as **Figure 13(c1)–(c3)** shows, the electric field close to the downward electrode tends to move up vertically, fostering the electron migration downward [36].

Furthermore, the impact of electron flux promotion on the charging of polyimide is addressed. Here, with four cases considered, we take the HV of 500 V and radiation time of 10 days for an example. It is shown in **Figure 14(a)** and **(b)** that

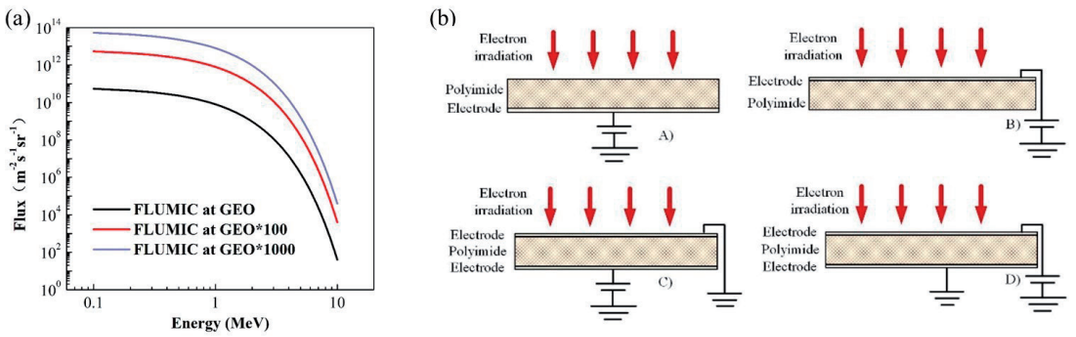

Figure 12.
(a) The FLUMIC model value at GEO environment. (b) Four cases of the sample [36].

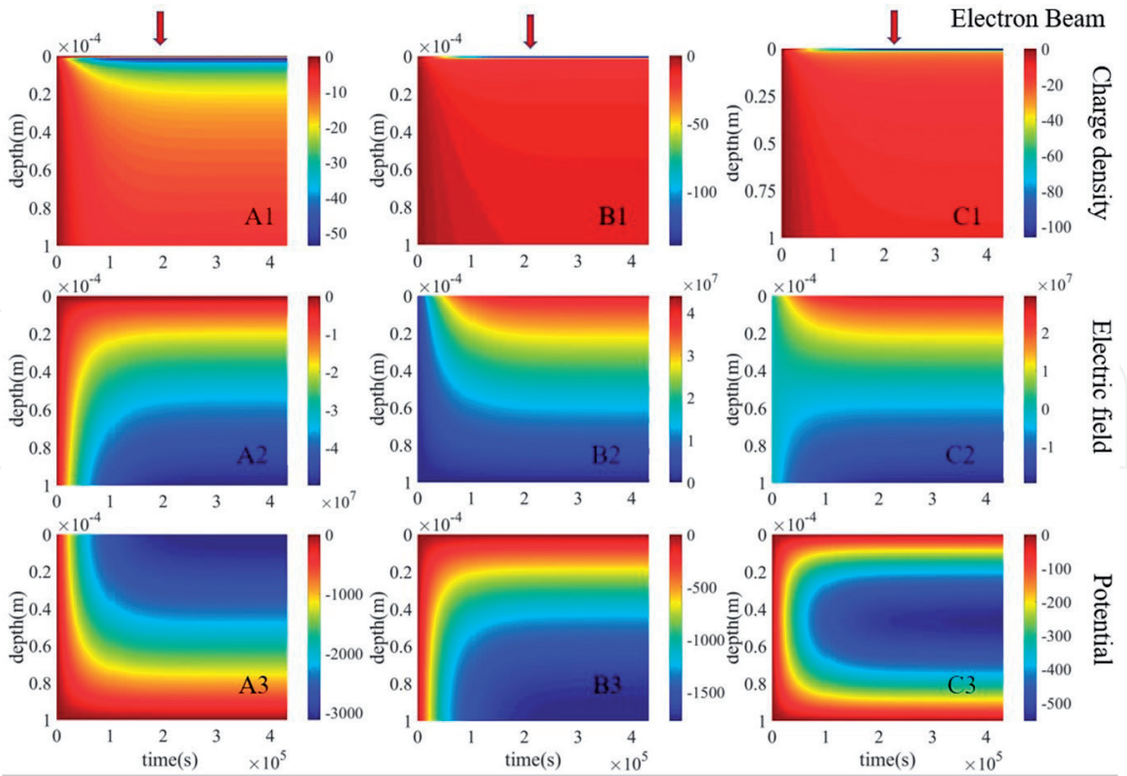

Figure 13.
Distribution of charge density, electric field and potential. (a) Suspended-grounded, (b) grounded-suspended, (c) grounded-grounded [36].

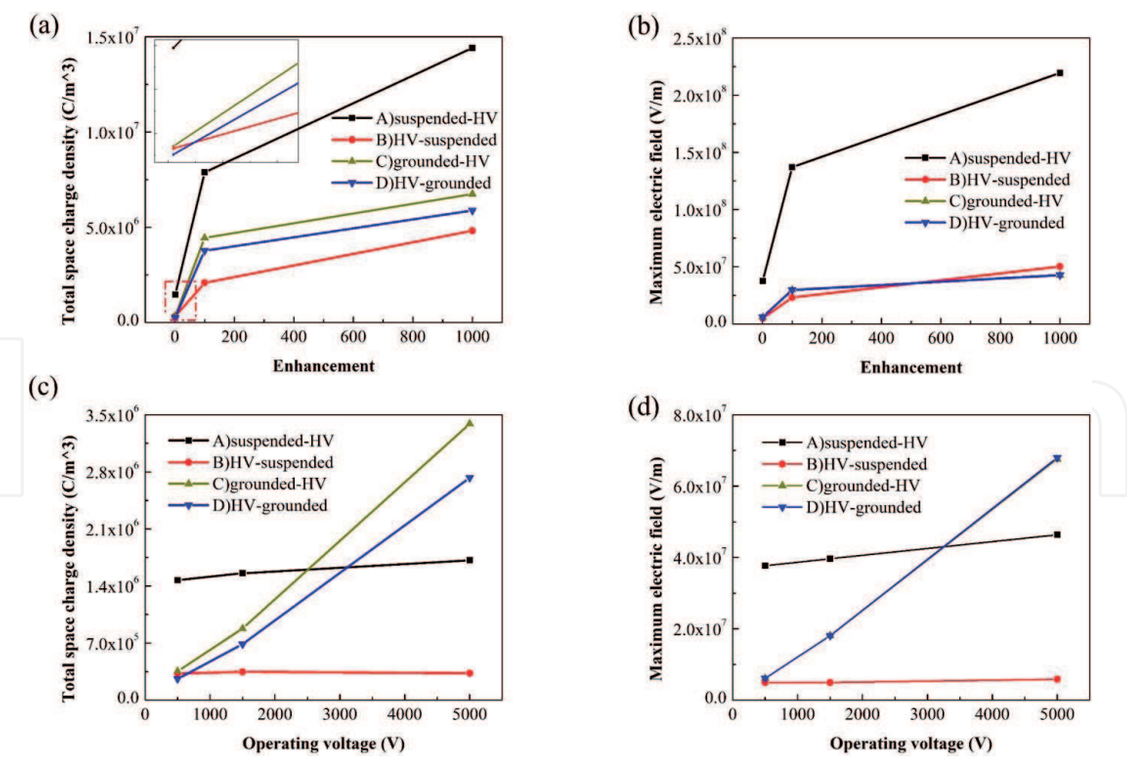

Figure 14.
(a) Influence of electron flux enhancement on total space charge density. (b) Influence of electron flux enhancement on maximum electric field. (c) Influence of operating voltage on total space charge density. (d) Influence of operating voltage on maximum electric field [36].

case A has the highest total space charge density and maximum electric field, which are significantly higher than those in other three cases at the same enhancement [36]. With flux enhancement increases, total space charge density reaches the valley

value under case D when enhancement is 1, while when enhancement increases to 100 and 1000, lowest charge density is seen in case B. Additionally, though charge density in cases B and D is varied, lines representing maximum electric field almost overlap. In case A, considering the voltage is applied to the lower electrode and electric field moves upward, accumulated electrons are attracted to the lower electrode; therefore, more electrons may be injected into the sample. On the contrary, in case B, the voltage is applied to upper electrode and electric field moves down; hence, vast charges are accumulated at the region near upper electrode, inhibiting further electron injection. In cases C and D, the electric field moves down and up at the region near upper and downward electrode, respectively. Based on the previous analysis, it can be determined that with an increase in flux enhancement, its impact on case A is more obvious than that in other cases.

At last, the influence of operating voltage on the charging of polyimide is discussed. Take the enhancement of 1 and the radiation time of 10 days as an example; we discuss the influence of operating voltage on the charging of polyimide in the four cases. As can be seen from **Figure 14(c)** and **(d)**, the increase of operating voltage has a small influence on cases A and B, since the virtual electrode is at infinity in both cases A and B [36].

6. Conclusions

Charging and discharging problem of polyimide in harsh space environment has been a major limit to the development of high-voltage and high-power spacecraft. Electrical and charge transport properties have great influences on the surface and deep charging-discharging characteristics. The conclusions drawn are as follows:

1. The parameters obtained from the electrical experiments can be used in the simulation of charge transport process, such as permittivity, trap energy level, trap density, the activation energy and so on. The electrical breakdown field decreases with an increase in sample thickness in the form of an inverse power function. The elongation of free volume caused by the displacement of the molecular chain associated with the accumulation of space charges and the distortion of electric field may play important roles in the breakdown characteristics of polyimide.

2. In terms of the surface electron properties of polyimide under electron radiation, the electrons deposited in dielectric surface layer will form a reverse electric field, which has a great impact on the dynamic process of the secondary electron movement and the process of deposition, transport and accumulation of electrons in the dielectric surface layer. In terms of charge transport properties in polyimide surface layer, the electrons deposited in dielectric surface layer will migrate to the inside under the action of the RIC. The charge conduction velocity is much lower than that of deposition, so the charge will continuously accumulate in the surface layer, which will cause a reaction force on kinetic electrons flowing to the dielectric surface.

3. Negative surface charge accumulation can increase the flashover voltage, to some extent. Since kinetic incident electrons in the vicinity of the CTJ can initiate the surface flashover at a much lower voltage, the shield of the spacecraft is of great importance. If a trade-off must be made on the shielding layer, the region of CTJ should be ensured. Moreover, narrow and deep gap between the electrodes can shield the kinetic incident electrons with non-normal incidence and may promote the surface flashover voltage.

4. The use of the suspended-HV insulation should be limited to reduce the influence of electron flux enhancement when designing a spacecraft. To increase the operating voltage of a large spacecraft like SSPS in the future, the rapid increase of space charge density and maximum electric field in grounded-HV and HV-grounded cases should be further considered.

Acknowledgements

This work was supported by the National Natural Science Foundation of China (NSFC) under Project with No. 51337008, the National Basic Research Program of China (973 Program) under Project with No. 2015CB251003, and NSFC under Projects with Nos. 11575140, 11275146, 51323012 and 51221005.

Conflict of interest

The authors declare no conflict of interest.

Author details

Xiaoping Wang, Daomin Min* and Shengtao Li*
State Key Laboratory of Electrical Insulation and Power Equipment, School of Electrical Engineering, Xi'an Jiaotong University, Xi'an, Shaanxi, China

*Address all correspondence to: forrestmin@xjtu.edu.cn and sli@xjtu.edu.cn

References

[1] Koons H, Mazur J, Selesnick R. The impacts of the space environment on space systems. In: Proceedings of the 6th Spacecraft Charging Conference; 1 September 2000; Hanscom. 2000. pp. 7-11

[2] Lai S. Fundamentals of Spacecraft Charging: Spacecraft Interactions with Space Plasma. 1st ed. Princeton University Press: Princeton; 2011. p. 272 DOI: 10.1515/9781400839094

[3] Wang L, Hou X. Key technologies and some suggestions for the development of space solar power station (in Chinede). Spacecraft Environment Engineering. 2014;**31**:343-350. DOI: 10.3969/j.issn.1673-1379.2014.04.001

[4] Sessler G, Hahn B, Yoon D. Electrical conduction in polyimide films. Journal of Applied Physics. 1986;**60**:318-326. DOI: 10.1063/1.337646

[5] Li G, Li S, Min D. Deep dielectric charging characteristics of ring structure irradiated by energetic electrons. IEEE Transactions on Dielectrics and Electrical Insulation. 2015;**22**:2349-2357. DOI: 10.1109/TDEI.2015.004840

[6] Ohya K, Inai K, Kuwada H. Dynamic simulation of secondary electron emission and charging up of an insulating material. Surface and Coatings Technology. 2008;**202**:5310-5313. DOI: 10.1016/j.surfcoat.2008.06.008

[7] Davies R, Dennison J. Evolution of secondary electron emission characteristics of spacecraft surfaces. Journal of Applied Physics. 1986;**60**: 318-326. DOI: 10.1063/1.337646

[8] Hodges J, Dennison J, Dekany J. In situ surface voltage measurements of dielectrics under electron beam irradiation. IEEE Transactions on Plasma Science. 2014;**42**:255-265. DOI: 10.1109/TPS.2013.2291862

[9] Fujii H, Okumura T, Takahashi M. Low-energy electron beam induced charging and secondary electron emission properties of fep film used on satellite surfaces. Electrical Engineering in Japan. 2014;**188**:9-17. DOI: 10.1002/eej.22501

[10] Fitting H, Touzin M. Secondary electron emission and self-consistent charge transport in semi-insulating samples. Journal of Applied Physics. 2011;**110**:44111. DOI: 10.1063/1.3608151

[11] Le R, Baudoin F, Griseri V. Charge transport modelling in electron-beam irradiated dielectrics: A model for polyethylene. Journal of Physics D: Applied Physics. 2010;**43**:315402. DOI: 10.1088/0022-3727/43/31/315402

[12] Perrin C, Griseri V, Inguimbert C. Analysis of internal charge distribution in electron irradiated polyethylene and polyimide films using a new experimental method. Journal of Physics D: Applied Physics. 2008;**41**:205417. DOI: 10.1088/0022-3727/41/20/205417

[13] Baudoin F, Le R, Teyssedre G. Bipolar charge transport model with trapping and recombination: An analysis of the current versus applied electric field characteristic in steady state conditions. Journal of Physics D: Applied Physics. 2008;**41**:25306. DOI: 10.1088/0022-3727/41/2/025306

[14] Sessler G, Figueiredo M, Leal FG. Models of charge transport in electron-beam irradiated insulators. IEEE Transactions on Dielectrics and Electrical Insulation. 2004;**11**:192-202. DOI: 10.1109/TDEI.2004.1285887

[15] Miller HC. Flashover of insulators in vacuum: the last twenty years.

IEEE Transactions on Dielectrics and Electrical Insulation. 2015;**22**:3641-3657. DOI: 10.1109/TDEI.2015.004702

[16] Li G, Li S, Pan S. Effect of electron irradiation on dc surface flashover of polyimide in vacuum. IEEE Transactions on Dielectrics and Electrical Insulation. 2016;**23**:1846-1853. DOI: 10.1109/TDEI.2016.005429

[17] Mengu C, Daniel E. Dielectric charging processes and arcing rates of high voltage solar arrays. Journal of Spacecraft and Rockets. 1991;**28**: 698-706. DOI: 10.2514/3.26302

[18] Zha J, Dang Z, Song H. Dielectric properties and effect of electrical aging on space charge accumulation in polyimide/tio2 nanocomposite films. Journal of Applied Physics. 2010;**108**:94113. DOI: 10.1063/1.3506715

[19] Matsui K, Tanaka Y, Takada T. Space charge behavior in low density polyethylene at pre-breakdown. IEEE Transactions on Dielectrics and Electrical Insulation. 2005;**12**:406-415. DOI: 10.1109/TDEI.2005.1453444

[20] Laurent C, Teyssedre G, Le R. Charge dynamics and its energetic features in polymeric materials. IEEE Transactions on Dielectrics and Electrical Insulation. 2013;**20**:357-381. DOI: 10.1109/TDEI.2013.6508737

[21] Takada T, Hayase Y, Tanaka Y. Space charge trapping in electrical potential well caused by permanent and induced dipoles for ldpe/mgo nanocomposite. IEEE Transactions on Dielectrics and Electrical Insulation. 2008;**15**:152-160. DOI: 10.1109/T-DEI.2008.4446746

[22] Henry B, Albert C, Joseph H. Guide to Mitigating Spacecraft Charging Effects. Jet Propulsion Laboratory California Institute of Technology; Hoboken NJ: Wiley; 2012. p. 196. DOI: 10.1002/9781118241400

[23] Li G, Min D, Li S. Research of deep dielectric charging characteristics of polytetrafluoroethene irradiated by energetic electrons. Acta Physica Sinica. 2014;**63**:454-461. DOI: 10.7498/aps.63.209401

[24] Tafazoli M. A study of on-orbit spacecraft failures. Acta Astronautica. 2009;**64**:195-205. DOI: 10.1016/j.actaastro.2008.07.019

[25] Xie F. Several global satellites in orbit failed in 2008. Satellite TV & IP Multimedia. 2009;**3**:20-21. DOI: CNKI:SUN:WSDS.0.2009-03-006

[26] Henry B. The charging of spacecraft surfaces. Reviews of Geophysics and Space Physics. 1981;**19**:577-616. DOI: 10.1029/RG019i004p00577

[27] Henry B, Albert C. Spacecraft charging, an update. IEEE Transactions on Plasma Science. 2001;**28**:2017-2028. DOI: 10.1109/27.902229

[28] Lai ST. A critical overview on spacecraft charging mitigation methods. IEEE Transactions on Plasma Science. 2003;**31**:1118-1124. DOI: 10.1109/TPS.2003.820969

[29] Min D, Li Y, Yan C. Thickness-dependent dc electrical breakdown of polyimide modulated by charge transport and molecular displacement. Polymers. 2018;**10**:1012. DOI: 10.3390/polym10091012

[30] Turnhout J. Thermally stimulated discharge of electrets. In: Sessler G, editor. Electrets. 2nd ed. Springer-Verlag: Berlin; 1987. pp. 81-215. DOI: 10.1007/3540173358_11

[31] Li G, Li S, Pan S. Dynamic charge transport characteristics in polyimide surface and surface layer under low-energy electron radiation. IEEE Transactions on Dielectrics and Electrical Insulation. 2016;**23**:2393-2403. DOI: 10.1109/TDEI.2016.7556518

[32] Sonnonstine T, Perlman M. Surface-potential decay in insulators with field-dependent mobility and injection efficiency. Journal of Applied Physics. 1975;**46**:3975-3981. DOI: 10.1063/1.322148

[33] Min D, Cho M, Khan AR. Surface and volume charge transport properties of polyimide revealed by surface potential decay with genetic algorithm. IEEE Transactions on Dielectrics and Electrical Insulation. 2012;**19**:600-608. DOI: 10.1109/TDEI.2012.6180255

[34] Chadband W. Electrical degradation and breakdown in polymers. IEE Review. 1992;**38**:11-12. DOI: 10.1049@ir19920168

[35] Li S, Pan S, Li G. Influence of electron beam irradiation on dc surface flashover of polyimide in vacuum. IEEE Transactions on Dielectrics and Electrical Insulation. 2017;**24**:1288-1294. DOI: 10.1109/TDEI.2017.006103

[36] Pan S, Min D, Wang X. Effect of electron irradiation and operating voltage on the deep dielectric charging characteristics of polyimide. IEEE Transactions on Nuclear Science. 2019;**66**:549-556. DOI: 10.1109/TNS.2018.2889167

[37] Wrenn G, Rodgers D, Buehler P. Modeling the outer belt enhancements of penetrating electrons. Journal of Spacecraft and Rockets. 2000;**37**: 408-415. DOI: 10.2514/2.3575

[38] Rodgers D. The FLUMIC electron environment model. In: Proceedings of the 8th Spacecraft Charging Technology Conference; 20-24 October 2003; Huntsville, Alabama. 2003. pp. 846-858